Experimental evidence of a collinear antiferromagnetic ordering in the frustrated $CoAl_2O_4$ spinel

B. Roy,[1] Abhishek Pandey,[1] Q. Zhang,[1] T. W. Heitmann,[2] D. Vaknin,[1] D. C. Johnston,[1] and Y. Furukawa[1]

[1]*Ames Laboratory and Department of Physics and Astronomy, Iowa State University, Ames, Iowa 50011, USA*

[2]*The Missouri Research Reactor Center, University of Missouri, Columbia, Missouri 65211, USA*

(Received 23 August 2013; revised manuscript received 21 September 2013; published 18 November 2013)

Nuclear magnetic resonance (NMR), neutron diffraction (ND), x-ray diffraction, magnetic susceptibility χ, and specific-heat measurements on the frustrated A-site spinel $CoAl_2O_4$ compound reveal a collinear antiferromagnetic ordering below $T_N = 9.8(2)$ K. A high-quality powder sample characterized by x-ray diffraction that indicates a relatively low Co-Al inversion parameter $x = 0.057(20)$ in $(Co_{1-x}Al_x)[Al_{2-x}Co_x]O_4$, shows a broad maximum around 15 K in $\chi(T)$ and a sharp peak at T_N in heat capacity C_p. The average-ordered magnetic moment of Co^{2+} ($S = \frac{3}{2}$) ions at the A site is estimated to be 2.4(1) μ_B from NMR and 1.9(5) μ_B from ND which are smaller than the expected value of 3 μ_B for $S = \frac{3}{2}$ and $g = 2$. Antiferromagnetic spin fluctuations and correlations in the paramagnetic state are revealed from the χ, NMR, and ND measurements, which are due to spin frustration and site inversion effects in the system. The ND data also show short-range dynamic magnetic ordering that persists to a temperature that is almost twice T_N.

DOI: 10.1103/PhysRevB.88.174415 PACS number(s): 75.10.Jm, 75.30.Cr, 76.60.−k, 78.70.Nx

I. INTRODUCTION

The investigation of magnetism in the insulating A-site spinel-structure compound $CoAl_2O_4$ has a long history which started with a suggestion of long-range antiferromagnetic (AFM) ordering below 4 K from magnetic susceptibility χ and neutron diffraction (ND) measurements performed by Roth.[1] The magnetism of this system originates from Co^{2+} ions $[(e_g)^4(t_{2g})^3]$ with spin $S = \frac{3}{2}$ at the tetrahedral A sites which form a diamond lattice (Fig. 1). The general formula for a normal oxide spinel compound is $A[B_2]O_4$ where the A and B atoms occupy the tetrahedral and octahedral holes between nearly cubic-close-packed O layers perpendicular to the [111] direction. Later on, the interest shifted to the spin frustration effects in the A-site spinel compounds after the ground state of the diamond lattice AFM was investigated theoretically.[2] The diamond lattice is composed of two interpenetrating face-centered-cubic (fcc) sublattices as shown in Fig. 1. The frustration is caused by the next-nearest-neighbor AFM interaction J_2 which couples nearest-neighbor sites of each fcc sublattice of the diamond structure, while the nearest-neighbor interaction J_1 between the two fcc sublattices alone does not induce any frustration for AFM ordering (Fig. 1).

Bergman *et al.*[2] pointed out theoretically that the ground state of the diamond lattice is a Néel-type antiferromagnet for a ratio of $J_2/J_1 < \frac{1}{8} = 0.125$. The ground state changes to a spiral spin-liquid state for $J_2/J_1 > \frac{1}{8}$. J_1 and J_2 for $CoAl_2O_4$ are reported to be $J_1 = 0.92(1)$ meV $\approx$ 10.67 K and with $J_2 = 0.101(2)$ meV $\approx$1.17 K, $J_2/J_1 = 0.11$.[3] Since the ratio is close to the critical ratio of $J_2/J_1 = \frac{1}{8}$, $CoAl_2O_4$ is considered to be located in the critical region between the AFM and the spiral spin-liquid states.

Experimental observations of the ground state of $CoAl_2O_4$ are contradictory. Tristan *et al.*[4] reported from χ and heat-capacity C_p measurements on powder samples that a spin-glass state is realized below 4.8 K with a high frustration parameter[5] $f = |\theta_{CW}|/T_M = 22$, where θ_{CW} is the Curie-Weiss temperature in the Curie-Weiss law and T_M is the spin-glass transition temperature. On the other hand, Suzuki *et al.* proposed a possible spin-liquid ground state below 9 K (Ref. 6) with $f = |\theta_{CW}|/T^* = 10$ where T^* is defined as the temperature at which a broad peak of C_p is observed. Zaharko *et al.* suggested an unconventional magnetically ordered phase in which the spin-liquid correlations were observed from neutron powder diffraction[7] (below 5 K) and single-crystal ND experiments[3] (below 8 K). MacDougall *et al.* also carried out a ND experiment on a single crystal of $CoAl_2O_4$ which showed a sharp cusp at 6 K in the T dependence of χ and an AFM state below 6.5 K.[8] They observed strong diffusive scattering in the AFM state where the phase transition was suggested to be first-order nature.[8] The origin of this ambiguity is probably site inversion, as has been pointed out by Zaharko *et al.*[3] The degree of site inversion between the A and B sites is usually defined by an inversion parameter x in the formula $A_{1-x}B_x[B_{2-x}A_x]O_4$, which here corresponds to $(Co_{1-x}Al_x)[Al_{2-x}Co_x]O_4$. The x value depends delicately on the method of sample preparation. The x values of the polycrystalline samples reported by Suzuki *et al.*, Tristan *et al.*,[4,9] and Zaharko *et al.*[7] are 0.04(1), 0.08–0.104, and 0.17, respectively. The x values for the single-crystal samples studied by Zaharko[3] and MacDougall[8] are 0.08 and 0.02(4), respectively.

Quite recently, Hanashima *et al.*[10] carried out a systematic study of the effects of site inversion on the magnetic properties of $(Co_{1-x}Al_x)[Al_{2-x}Co_x]O_4$ where x is controlled from 0.0467 to 0.153 by changing the heat treatment conditions. The $\chi(T)$ of the sample with the lowest x value $x = 0.0467$ shows a broad maximum at 14 K and does not show any signature of magnetic ordering down to 2 K, similar to that reported by Suzuki *et al.*,[6] suggesting a spin-liquid state. With increasing x, the broad maximum moves to lower temperature (10 K for $x = 0.0643$), and for $x > 0.101$, a clear cusp in the T dependence of χ is observed which is attributed to a spin-glass transition below $T_g \approx 4.5$ K. In the intermediate region $0.0791 < x < 0.847$, a coexistence of the spin-liquid state and spin-glass state is proposed. Hanashima *et al.* conclude that with increasing x the spin-liquid state collapses and the spin-glass order emerges for $x > 0.101$.

It is important to understand whether the intrinsic ground state of $CoAl_2O_4$ for small values of x is a spin-glass state, an antiferromagnet, or a spin-liquid state due to the spin frustration. To investigate the ground state of $CoAl_2O_4$

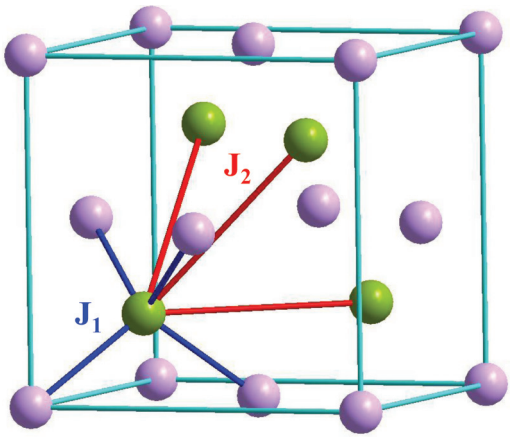

FIG. 1. (Color online) Diamond lattice formed by Co atoms of cubic spinel $CoAl_2O_4$, composed of two interpenetrating face-centered-cubic (fcc) sublattices shown by purple and green spheres. The nearest-neighbor interaction J_1 between the two fcc sublattices and the next-nearest-neighbor interaction J_2 within the same fcc sublattice is shown.

one needs a high-quality sample with a small value of the inversion parameter x. In this paper, we report measurements of crystallography, magnetization, χ, specific heat, nuclear magnetic resonance (NMR), and ND on a well-characterized polycrystalline $CoAl_2O_4$ sample with inversion parameter $x = 0.057(20)$. We conclude that $CoAl_2O_4$ exhibits collinear AFM ordering below the $T_N = 9.8(2)$ K, with an ordered moment of 2.4(1) μ_B from NMR and 1.9(5) μ_B from ND measurements.

II. EXPERIMENTAL DETAILS

A polycrystalline sample of $CoAl_2O_4$ was synthesized by the solid-state reaction method using Co_3O_4 (99.9985%) and Al_2O_3 (99.995%) from Alfa Aesar as the starting materials. As a precautionary measure to check the phase purity of the starting materials, room-temperature x-ray diffraction (XRD) measurement was performed on the Co_3O_4 starting material. The results revealed that the material was not single phase and with a sizable presence of binary CoO. The weight fraction of CoO obtained by two-phase Rietveld refinement of the powder XRD pattern was 1.4(1)%. The molar fraction of CoO in Co_3O_4 was considered while calculating the stoichiometry of cobalt in the starting mixture. Stoichiometric mixtures of Co_3O_4 and Al_2O_3 were thoroughly mixed and pressed into a pellet. The pressed pellet was placed inside an alumina crucible and heated to 875 °C in 20 h, held there for 40 h, and then cooled to 500 °C in 100 h and held there for 80 h, and finally the sample was cooled by switching off the furnace. The material was then thoroughly reground and repressed into a pellet. The pellet was placed in the same alumina crucible and heated to 1000 °C in 20 h, held there for 50 h, then cooled to 700 °C in 60 h, held there for 2 h, and finally slowly cooled to 400 °C in 100 h and held there for 100 h. At this time, the furnace was switched off and the sample cooled to room temperature. The sample was Persian blue in color.

Structural characterization of the sample was performed at room temperature using powder XRD data obtained from a Rigaku Geigerflex powder x-ray diffractometer utilizing CuK_α radiation. The FULLPROF package[11] was used in the Rietveld XRD data refinement. Temperature-dependent and applied magnetic field H-dependent magnetic measurements were performed using a magnetic properties measurement system (MPMS, Quantum Design, Inc.). Heat capacity C_p was measured by the thermal relaxation method using a physical properties measurement system (PPMS, Quantum Design, Inc.).

NMR measurements were conducted by probing the ^{27}Al nuclei ($I = 5/2$, $\gamma/2\pi = 11.09375$ MHz/T, $Q = 0.149$ barns) and the ^{59}Co nuclei ($I = 7/2$, $\gamma/2\pi = 10.03$ MHz/T, $Q = 0.4$ barns) by using a phase-coherent spin-echo pulse spectrometer. The NMR spectrum was taken by recording the spin-echo signal intensity while sweeping the external magnetic field at a fixed resonance frequency. The Co NMR spectrum under zero magnetic field was obtained by plotting the spin-echo intensity point by point at different fixed frequencies.

Neutron diffraction measurements were performed using the triple-axis spectrometer (Triax) at the University of Missouri Research Reactor (MURR). Approximately 2 g of $CoAl_2O_4$ powder were loaded into a vanadium sample cell and mounted on the cold head of an Advanced Research Systems closed-cycle refrigerator on Triax. Powder ND patterns were obtained on the spectrometer operated with a Cu(220) monochromator at a wavelength of 1.348 Å, a PG(002) analyzer set at the elastic position, and collimation of $60' - 40' - 40' - 80'$. Sapphire and Si filters were used upstream from the monochromator and none after the sample. Additional scans with greater statistics were also obtained at the key positions in wave-vector (**q**) space corresponding to the putative spiral or collinear magnetic orderings. The 2-g sample held in the same holder was also measured on the MURR high-resolution neutron powder diffractometer (PSD), which utilizes a double-focusing perfect single Si monochromator at the (511) reflection to illuminate the sample with 1.4805-Å wavelength neutrons. Diffracted neutrons are detected by five linear position-sensitive detectors. The sample temperature was adjusted with a Leybold closed-cycle refrigerator with an 18-K base temperature.

III. CRYSTALLOGRAPHY

As described in Sec. I, it was shown that the magnetic properties of $CoAl_2O_4$ depend delicately on the amount of site inversion present in the sample.[10] The goal in this work is to investigate the magnetic properties of a high-quality polycrystalline sample of $CoAl_2O_4$ having minimal site inversion. To achieve this, we synthesized a polycrystalline sample of $CoAl_2O_4$ using the controlled thermal treatments described in the previous section. However, we could not achieve a completely site-inversion-free sample. Rietveld analysis of the room-temperature powder XRD data of our sample showed a minor amount of site inversion corresponding to the formula $(Co_{1-x}Al_x)[Al_{2-x}Co_x]O_4$. The goodness-of-fit parameter χ^2 obtained by single-phase Rietveld refinements of the room-temperature powder XRD data versus site inversion x is shown in Fig. 2(a). From this figure we estimate $x = 0.057(20)$. This value of x is slightly smaller than that reported by Tristan *et al.* (0.080–0.104) in Refs. 4 and 9 and Zaharko *et al.* (0.08)

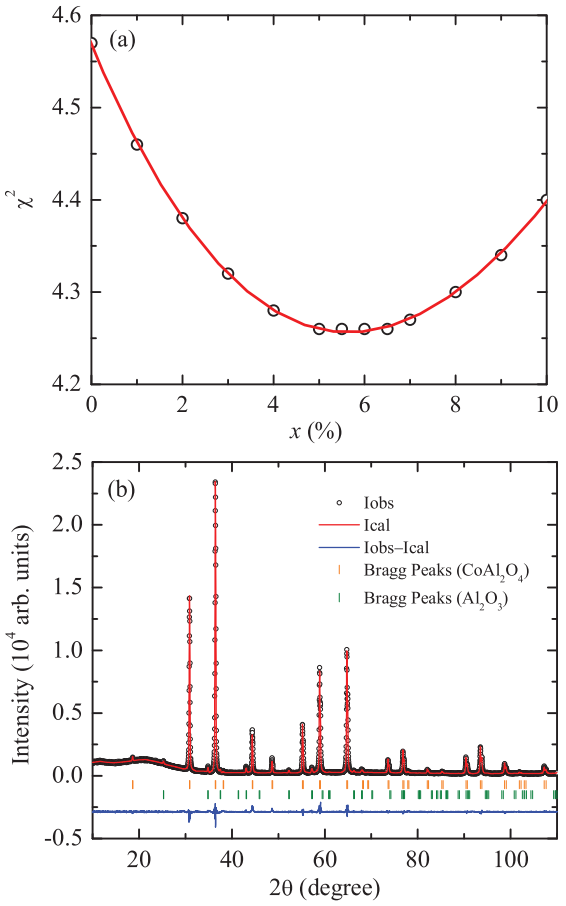

FIG. 2. (Color online) (a) Goodness-of-fit parameter χ^2 versus site inversion parameter x obtained by single-phase Rietveld refinement of our polycrystalline $CoAl_2O_4$ sample. The red line is shown as eye guides. (b) Room-temperature powder x-ray diffraction data, two-phase Rietveld refinement, Bragg positions, and difference profile for $CoAl_2O_4$ and the Al_2O_3 impurity phase.

in Ref. 3, and is equal, within error bars, to that reported by Suzuki *et al*. (0.04) in Ref. 6 and Hanashima *et al*. (0.0467).[10]

Additionally, powder XRD data showed the presence of a minor secondary phase Al_2O_3 in our sample. After estimating the site inversion parameter by single-phase Rietveld refinement, we performed a two-phase Rietveld refinement with a fixed value of $x = 0.057$. Figure 2(b) shows the results of the two-phase Rietveld refinement. We achieved an excellent fit to the data, and the calculated weight fraction of Al_2O_3 was 3.5(2)%. The crystal and Rietveld refinement quality parameters are listed in Table I.

TABLE I. Crystal data, Wyckoff positions, and refined structural parameters along with the Rietveld refinement quality parameters for $CoAl_2O_4$ obtained by two-phase Rietveld refinement of the room-temperature powder x-ray diffraction data. The χ^2 value is smaller than in Fig. 2(a) because those were single-phase fit, not taking into account the peaks from the Al_2O_3 impurity phase.

Structure	Spinel ($MgAl_2O_4$ type)
Space group	$Fd\bar{3}m$ (No. 227)
Lattice parameter	8.1011(2) Å
$CoAl_2O_4$ weight fraction	96.5(2)%
Inversion parameter (x)	0.057(20)
Atom	Wyckoff positions
Co	$8a$ $(\frac{1}{8},\frac{1}{8},\frac{1}{8})$
Al	$16d$ $(\frac{1}{2},\frac{1}{2},\frac{1}{2})$
O	$32e$ (x_O,x_O,x_O) where $x_O = 0.2630(1)$
Refinement quality parameters	
χ^2	2.49
R_p (%)	4.69
R_{wp} (%)	6.37

IV. MAGNETIZATION AND MAGNETIC SUSCEPTIBILITY

Isothermal magnetization M versus H data of our polycrystalline $CoAl_2O_4$ sample at four different temperatures are shown in Fig. 3. The $M(H)$ data at $T = 10,100$, and 300 K are proportional to H in the entire field range of measurement. However, the $M(H)$ data at 1.8 K show nonlinear behavior with positive curvature in the entire field range of measurement. This behavior is typical of Heisenberg AFMs with anisotropy as observed from the ND measurements.[3]

The $\chi(T)$ of our sample measured under zero-field-cooled (ZFC) and field-cooled (FC) conditions in the presence of an applied magnetic field $H = 1$ T is shown in Fig. 4. The $\chi(T)$ exhibits a broad maximum centered at $T = 15(1)$ K suggesting the presence of AFM correlations in the material. The ZFC and FC $\chi(T)$ data nearly overlap in the entire temperature range of measurement [inset (a), Fig. 4], which is consistent with the result on polycrystalline $CoAl_2O_4$ reported by Suzuki *et al*. with a low-inversion parameter $x = 0.04(2)$.[6] Our $\chi(T)$ data are also consistent with the results for the $x = 0.0467$ sample of Hanashima *et al*.,[10] except below 9.6 K where there is a rather significant bifurcation of ZFC and FC data in their sample. As discussed in Sec. I, it has been shown in previous reports that the low-temperature magnetic properties of $CoAl_2O_4$ are very sensitive to the amount of site inversion between the A and the B sites in the samples. Samples with relatively large inversion parameters ($x \geqslant 0.08$) have been reported to show

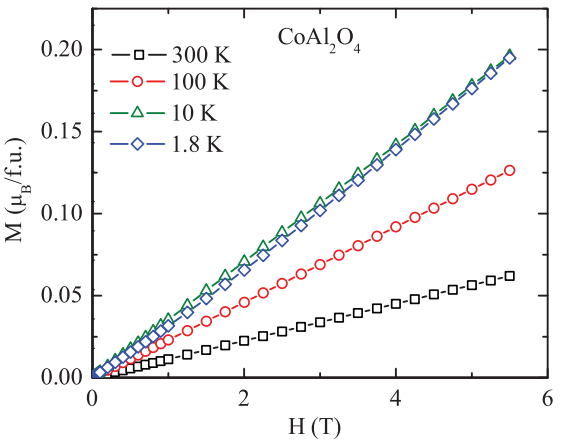

FIG. 3. (Color online) Isothermal magnetization M versus applied magnetic field H for $CoAl_2O_4$ measured at four different temperatures between 1.8 and 300 K.

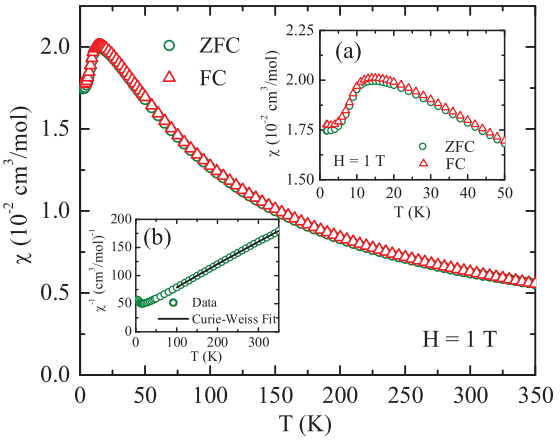

FIG. 4. (Color online) Zero-field-cooled (ZFC) and field-cooled (FC) magnetic susceptibility χ versus temperature T for $CoAl_2O_4$. The ZFC and FC data nearly overlap each other in the entire T range of measurement. Inset (a): Expanded plot of $\chi(T)$ below 50 K. Inset (b): Inverse magnetic susceptibility χ^{-1} versus T. Solid line is Curie-Weiss fit to the data as described in the text.

spin-glass-like behaviors,[4] while samples with $x \leqslant 0.05$ have been argued to have spin-liquid ground states.[6,10]

The $\chi(T)$ data between 100 and 350 K were fitted by the Curie-Weiss law [inset (b) in Fig. 4]

$$\chi(T) = \frac{C}{T - \theta_{CW}} + \chi_0, \tag{1}$$

where C is the Curie constant and χ_0 is the T-independent orbital contribution to χ. The fitted value of χ_0 is $6(2) \times 10^{-4}$ cm^3/mol, which is in good agreement with Van Vleck susceptibility $4(2) \times 10^{-4}$ cm^3/mol for Co^{2+} ions at the A site estimated from NMR measurements as will be described in Sec. VI B. This value is almost one order of magnitude greater than the diamagnetic susceptibility $\chi_{dia} = -7.4 \times 10^{-5}$ cm^3/mol estimated from the reference compound $ZnAl_2O_4$ (Ref. 4). The fitted values of C, θ_{CW}, and the effective moment μ_{eff} and g factors determined from C are listed in Table II. For comparison, parameters for some other $CoAl_2O_4$ samples reported in the literature are also included in Table II. The C obtained for our sample is larger than the value 1.875 cm^{3}K/mol expected for spin $S = \frac{3}{2}$ and $g = 2$. However, our value of C is smaller than those reported in the literature for this material (Table II). If we consider that magnetism in $CoAl_2O_4$ is entirely due to Co^{2+} spins with $S = \frac{3}{2}$, then the calculated value of powder-averaged g factor is 2.12(5) which is again considerably smaller than that reported for $CoAl_2O_4$ in the literature (Table II) and $g = 2.26$ reported from electron spin resonance (ESR) measurements.[13] It should be noted, however, that C value strongly depends on χ_0. If one assumes $\chi_0 = 0$, then $C = 2.52(6)$ cm^{3}K/mol was obtained with $\theta_{CW} = -104(9)$ K (Table II). Using this value of C, the g factor is estimated to be 2.32(2) which is slightly larger than $g = 2.26$ obtained from the ESR measurements.[13] It appears that the value of the frustration parameter f depends sensitively on the degree of antisite disorder present in $CoAl_2O_4$ samples. The f value of our sample is lower than those reported in the literature (Table II).

V. HEAT CAPACITY

The C_p versus T for $CoAl_2O_4$ is shown in Fig. 5. Low-temperature $C_p(T)$ data of $CoAl_2O_4$ along with those of the nonmagnetic reference compound $ZnAl_2O_4$ (Ref. 9) are shown in the inset on an expanded scale. The $C_p(T)$ data of $CoAl_2O_4$ show a sharp peak centered at $T = 9.7(2)$ K suggesting a magnetic transition at this temperature. The magnetic contribution $C_{Mag}(T)$ to the total heat capacity was obtained by subtracting the $C_p(T)$ data of $ZnAl_2O_4$ from that of $CoAl_2O_4$ [Fig. 6(a)].

The magnetic entropy variation $\Delta S_{Mag}(T)$ was calculated from C_{Mag} using

$$\Delta S_{Mag}(T) = \int_0^T \frac{C_{Mag}(T)}{T} dT. \tag{2}$$

The T dependence of ΔS_{Mag} is shown in Fig. 6(b), where we have also indicated the expected high-temperature

TABLE II. Parameters obtained from magnetic susceptibility $\chi(T)$ data and their fit using high-temperature Curie-Weiss law described in the text for polycrystalline $CoAl_2O_4$. Data for some other $CoAl_2O_4$ samples reported in the literature have been included for comparison. The listed parameters in the table are site inversion parameter x, magnetic ordering temperature T_M, characteristic temperature for spin-liquid state T^*, Curie-Weiss temperature θ_{CW}, frustration parameter $f = |\theta_{CW}/T_M|$ or $|\theta_{CW}/T^*|$, Curie constant C, effective paramagnetic moment μ_{eff} obtained from C assuming $g = 2$, and effective spectroscopic splitting factor g obtained assuming $S = \frac{3}{2}$ for the Co^{2+} ions.

x (%)	T_M (K)	T^* (K)	θ_{CW} (K)	f	C (cm^{3}K/mol)	μ_{eff} (μ_B/f.u.)	g	Ground state	Ref.
			−73(8)	8(1)	2.1(1)	4.1(1)	2.12(5)		This work[a]
5.7(2.0)	9.8(2)		−104(9)	11(1)	2.52(6)	4.49(5)	2.32(3)	AFM	This work[b]
4(2)		9[c]	−89(6)	9.9(7)	2.5(1)	4.45(8)	2.30(4)	Spin liquid	6
4.67		9.6[d]	−93.0	9.7	2.38	4.36	2.25	Spin liquid	10
2(4)	6.5		−109(1)	18.0(2)	2.99(4)	4.89(3)	2.53(2)	AFM	8
8(3)	4.8(2)		−104(2)	22(1)	2.7(1)	4.65(9)	2.40(4)	Spin glass	4
8	8		−94(1)	12(1)	2.7(1)	4.63(2)	2.40(1)	Unconventional	3,12

[a]Estimated with $\chi_0 = 6(2) \times 10^{-4}$ cm^3/mol.
[b]Obtained assuming $\chi_0 = 0$.
[c]Determined from the peak position in the heat capacity.
[d]Defined by the temperature at which ZFC and FC susceptibilities deviate from each other.

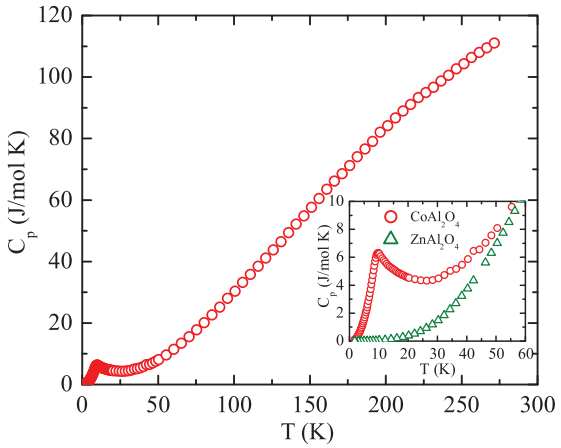

FIG. 5. (Color online) Heat capacity C_p versus temperature T for $CoAl_2O_4$. Inset: The $C_p(T)$ of $CoAl_2O_4$ at an expanded scale near magnetic transition temperature T_N along with $C_p(T)$ of the nonmagnetic analog compound $ZnAl_2O_4$ (Ref. 9). The plotted $C_p(T)$ data of $ZnAl_2O_4$ for $T > 10$ K are the experimental data of Ref. 9. The data below 10 K were obtained by extrapolating these data, using the function $C_p = \beta T^3$.

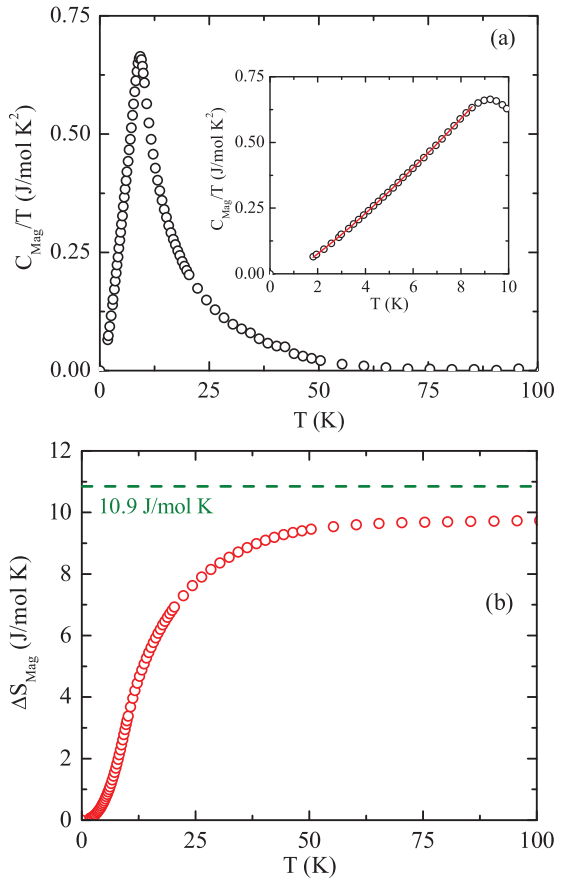

FIG. 6. (Color online) (a) Magnetic contribution to the heat capacity C_{Mag} over temperature T versus T. An additional data point $C_{Mag}/T = 0$ at $T = 0$ was inserted for better estimation of the magnetic entropy. Inset: C_{Mag}/T versus T below 10 K. Solid line shows $C_{Mag}/T \propto T^{1.23}$ dependence. (b) Magnetic entropy variation ΔS_{Mag} versus T. The horizontal dashed line represents the calculated high-T limit $S_{Mag} = 10.9$ J/mol K.

limit

$$S_{Mag}(T \to \infty) = (1-x)R\ln(2S+1) = 0.943R\ln 4 = 10.9\ \text{J/molK}, \quad (3)$$

where we consider only the contribution from the A-site Co^{2+} ions with $S = \frac{3}{2}$ for our sample with $x = 0.057$ for simplicity. From the $\Delta S_{Mag}(T)$ data presented in Fig. 6(b) we find that (i) ΔS_{Mag} does not reach the expected saturation limit and its value at 100 K is 9.74 J/mol K which is ≈11% smaller than 10.9 J/mol K. Considering the presence of ≈6% site inversion between Co and Al atoms in our sample, we can not rule out a somewhat magnetically disordered ground state in the material. Such a scenario would result in a nonzero S_{Mag} at $T = 0$ K, which could be the possible reason for the observed discrepancy between the calculated value of S_{Mag} $(T \to \infty)$ and the smaller value of $\Delta S_{Mag}(T)$ $(T \to \infty)$. (ii) The value of ΔS_{Mag} at $T_N = 9.7$ K is 3.11 J/mol K which is only ≈32% of its high-T value. This clearly shows that a major part of the magnetic entropy is released between 10 and 50 K, which indicates the persistence of strong dynamic short-range magnetic order above T_N up to approximately 50 K.

There are contradictory reports in the literature about the T dependence of C_p below the magnetic ordering temperature. While Tristan *et al.*[4] and MacDougall *et al.*[8] reported that C_p varies as T^2, Suzuki *et al.* find that this dependence is $T^{2.5}$.[6]

In our sample, we find that C_{Mag} below T_N follows $C_{Mag} \propto T^{2.23}$ which is approximately midway between the T^2 and $T^{2.5}$ power-law dependencies. Our observation is inconsistent with the linear T dependence of C_p expected for spin-glass systems[14,15] and the exponent is slightly lower than the $T^{7/3}$ dependence predicted by Bergman *et al.* for spiral spin-liquid frustrated diamond-lattice antiferromagnets.[2]

VI. NUCLEAR MAGNETIC RESONANCE

A. ^{27}Al-NMR

Figure 7 shows the field-swept ^{27}Al-NMR spectrum at $T = 25$ K and resonance frequency $\nu_0 = 9.3$ MHz. Since our sample

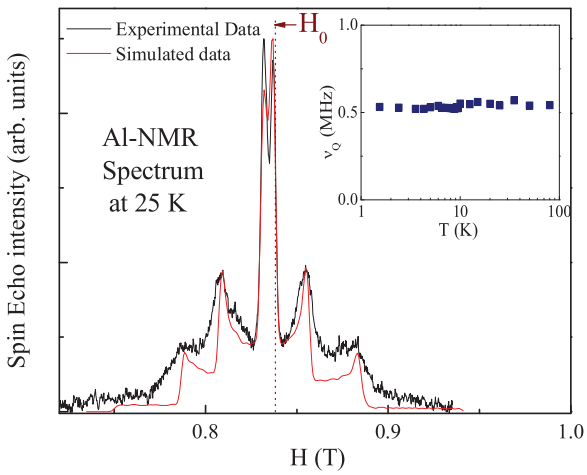

FIG. 7. (Color online) Field-swept ^{27}Al-NMR spectrum at 25 K and $\nu_0 = 9.3$ MHz. The red line shows the simulated spectrum with $\nu_Q = 0.55$ MHz and $\eta = 0$. The inset shows the temperature T independence of the quadrupole frequency ν_Q.

consists of grains with randomly oriented crystal axes, the spectrum is a powder pattern. The spectrum can be explained by a combination of a large Zeeman interaction $\mathcal{H}_Z$ and a small quadrupole interaction $\mathcal{H}_Q$. The nuclear spin Hamiltonian can therefore be expressed as

$$\mathcal{H} = \mathcal{H}_Z + \mathcal{H}_Q, \tag{4}$$

where $\mathcal{H}_Z = -\gamma\hbar H_0(1+K)I_z$ and $\mathcal{H}_Q = \frac{e^2qQ}{4I(2I-1)}[(3I_z^2 - I^2) + \frac{1}{2}\eta(I_+^2 + I_-^2)]$, Q is the quadrupole moment of the ^{27}Al nucleus, and K is the NMR shift which is a sum of isotropic (K_{iso}) and axial (K_{ax}) parts. η is the asymmetry parameter for the electric field gradient (EFG) defined by $\frac{\frac{\partial^2 V}{\partial X^2} - \frac{\partial^2 V}{\partial Y^2}}{\frac{\partial^2 V}{\partial Z^2}}$, $|\frac{\partial^2 V}{\partial Z^2}| > |\frac{\partial^2 V}{\partial Y^2}| > |\frac{\partial^2 V}{\partial X^2}|$, $eq = |\frac{\partial^2 V}{\partial Z^2}|$, and the quadrupole frequency $\nu_Q = \frac{3e^2qQ}{2I(2I-1)h}$. The z and Z axes are the quantization axes for the Zeeman and quadrupole interactions, respectively. The observed spectrum is well reproduced by a simulated spectrum shown by a red line in Fig. 7 with $\nu_Q = 0.55$ MHz and $\eta = 0$. The value of ν_Q is independent of T in the measured range of 1.8 to 300 K within our experimental uncertainty as shown in the inset of Fig. 7. In contrast, K_{iso} and K_{ax} show weak temperature dependencies. The weak T dependencies of the NMR shifts are consistent with previous data reported by Miyatani *et al.*[16] who measured the ^{27}Al-NMR spectrum in $CoAl_2O_4$ with the continuous-wave NMR method above 77 K, although the K_{ax} component was not detected in the previous measurement.

The T dependencies of K_{iso} and K_{ax} follow the T dependence of χ as shown in Fig. 8 where the NMR shifts are plotted as a function of χ with T as an implicit parameter. Here the NMR shifts are determined by measuring the NMR spectrum with a higher resonance frequency of 70.9 MHz to improve the accuracy. The NMR shift has contributions from the T-dependent spin part K_{spin} and a small T-independent orbital part K_0. $K_{spin}(T)$ is related to the spin susceptibility with hyperfine coupling constant A_{hf} as follows:

$$K(T) = K_0 + \frac{A_{hf}}{N_A}\chi(T), \tag{5}$$

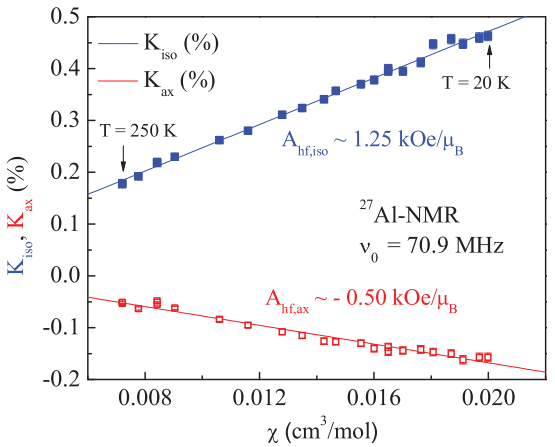

FIG. 8. (Color online) ^{27}Al-NMR shifts (K_{iso} and K_{ax}) versus χ with T as an implicit parameter. The solid lines show the linear fit using Eq. (5).

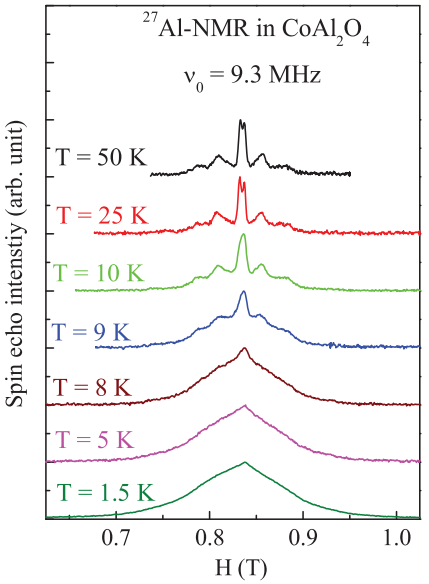

FIG. 9. (Color online) Field-swept ^{27}Al-NMR spectra at various temperatures with resonance frequency $\nu_0 = 9.3$ MHz.

where N_A is the Avogadro number. The isotropic ($A_{hf,iso}$) and axial ($A_{hf,ax}$) parts of the hyperfine coupling constants for the Al nucleus are evaluated from the slope of the K-χ plots (Fig. 8) to be 1.25(2) kOe/μ_B and $-0.50(2)$ kOe/μ_B, respectively, and K_0 is 0.023(4)% and 0.013(3)% for the isoisotropic and axial parts, respectively. Classical dipolar field calculations indicate that the hyperfine field can not be due to the classical dipolar field at the Al sites from neighboring Co^{2+} ($S = \frac{3}{2}$) spins, but is rather due to the transferred hyperfine field due to finite spin transfer from Co^{2+} spins. The anisotropy in the hyperfine field suggests that anisotropic orbitals such as the $2p$ and $3p$ orbitals on Al atoms are polarized by the spin transfer from the neighboring Co atoms.

The spectrum starts to broaden suddenly below ≈10 K, as shown in Fig. 9. The broadening indicates a static magnetic ordering of the Co^{2+} spins which produce a finite static internal field at the Al sites. The symmetric line broadening indicates an AFM state. Figure 10 shows the T dependence of the linewidth

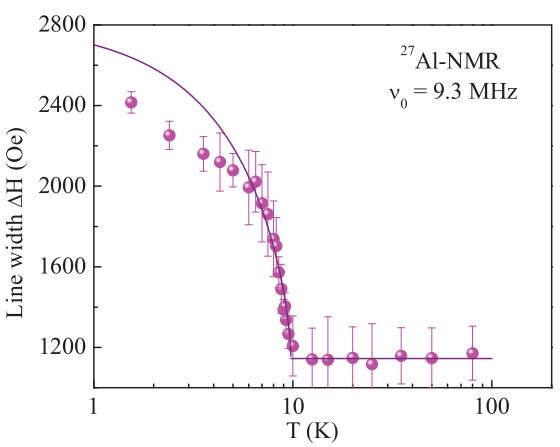

FIG. 10. (Color online) T dependence of the linewidth at 10% of the peak intensity. The solid purple line shows the fit by Eq. (6) using data in the temperature range of 7.5 K $< T <$ 10 K.

(ΔH) determined at 10% of the peak intensity. Since the broadening of the ^{27}Al-NMR linewidth in our polycrystalline sample below ≈10 K is produced by the Co^{2+} spin moments in the magnetically ordered state, the T dependence of the linewidth reflects that of the sublattice magnetization in the AFM state. The Néel temperature T_N is determined by fitting ΔH near T_N in Fig. 10 by

$$\Delta H(T) = \Delta H_0 \left(1 - \frac{T}{T_N}\right)^{\beta} + c, \qquad (6)$$

where $\Delta H_0 \approx 1669$ Oe and $c \approx 1145$ Oe is a constant determined by averaging the nearly T-independent ΔH above T_N. By fitting data in the temperature range of 7.5 K $< T <$ 10 K, by Eq. (6), T_N is estimated to be 9.8(2) K with $\beta = 0.65(5)$.

B. ^{59}Co-NMR

In the paramagnetic state at $T = 125$ K, we observe two peaks in the ^{59}Co-NMR spectrum as shown in Fig. 11. With decreasing T, the peak observed at $H \approx 6.9$ T shifts to higher magnetic field and the other peak at $H \approx 6.8$ T moves to slightly lower magnetic field. While the former peak disappeared below 10 K, the latter peak could be observed down to the lowest temperature of 1.5 K. These behaviors are very similar to ^{59}Co-NMR data for the magnetic Co^{2+} ($S = \frac{3}{2}$) at the A site and nonmagnetic low-spin Co^{3+} [$(t_{2g})^6(e_g)^0$, $S = 0$] at the B site in the spinel-structure antiferromagnet Co_3O_4 with $T_N = 34$ K.[17] Thus, the former signal, which vanishes due to very large internal field at the Co^{2+} site, can be assigned to be the Co at the tetrahedral A site and the latter signal can be attributed to the Co occupying the octahedral B site.

From the intensities of the Co signals occupying the A and the B sites, corrected by their respective longitudinal and transverse relaxation times (T_1 and T_2, respectively), we have evaluated the inversion parameter to be $x \approx 0.06(2)$. This value is in good agreement with that from the x-ray analysis. We notice that the T dependence and the magnitude of the NMR shift of the Co signal from the B sites in $CoAl_2O_4$ is very

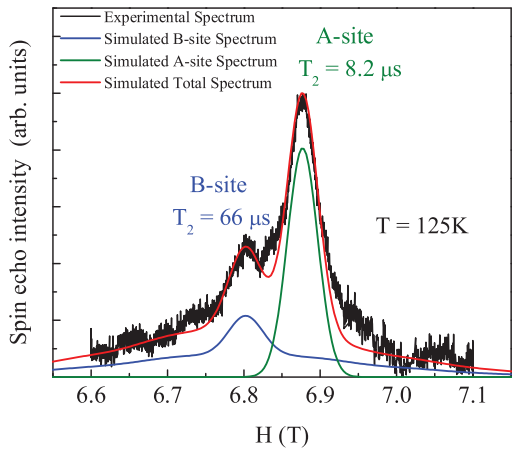

FIG. 11. (Color online) Field-swept ^{59}Co-NMR spectrum at $T = 125$ K and resonance frequency $\nu_0 = 70.2$ MHz. The two peaks correspond to the Co ions occupying the A site (magnetic Co^{2+} ion) and the B site (nonmagnetic Co^{3+} ion), respectively. The transverse relaxation time $T_2 = 8.2$ and 66 μs for the A and B sites, respectively.

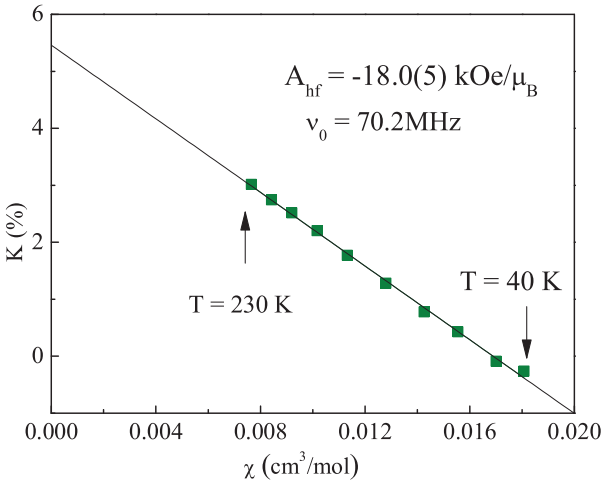

FIG. 12. (Color online) ^{59}Co-NMR shift K versus χ with T as an implicit parameter. The solid line is a linear fit.

close to that observed in the Co NMR signal from the B sites in Co_3O_4 where the Co^{3+} ions are in a nonmagnetic state with low spin $S = 0$.[17] From these results, we may consider that the Co ions occupying the B site in $CoAl_2O_4$ could be Co^{3+} with low spin state as in the case of Co ions at the B site in Co_3O_4. This could be possible if we assume that the deviation from oxygen stoichiometry exists as in $(Co_{1-x}Al_x)[Al_{2-x}Co_x]O_{4+\delta}$ to satisfy charge compensation of the compound. However, we can not rule out completely that the observed nonmagnetic Co is from an impurity phase, although it seems unlikely.

The hyperfine coupling constant of Co at the A site is estimated from the K-χ plot in Fig. 12 to be $-18.0(5)$ kOe/μ_B which is considerably smaller than the value of -105 kOe/μ_B for a free Co^{2+} ion. Such a small Co hyperfine coupling constant at the A site has been reported previously to be -18.3 kOe/μ_B and -15.7 kOe/μ_B in the antiferromagnetic Co_3O_4 ($T_N = 34$ K) (Ref. 17) and in ferrimagnetic $CoCr_2O_4$ ($T_C = 97$ K) (Ref. 18), respectively. The small coupling constant was well explained by taking the second-order orbital moment due to the spin-orbit interaction into consideration. Here, we present a similar discussion as in the previous papers.[17,18]

The major contributions to the magnetic hyperfine coupling constant at the ^{59}Co nucleus are dominated by the d-core polarization (A_{hf}^{core}), dipolar (A_{hf}^{dip}), and orbital (A_{hf}^{orb}) terms:[17–19]

$$A_{hf} = A_{hf}^{core} + A_{hf}^{dip} + A_{hf}^{orb}. \qquad (7)$$

Due to the crystal-field effect, the ground state of the $Co^{2+}(d^7)$ ion occupying the tetrahedral A site has four electrons in the two lower e_g orbitals and three in the upper three t_{2g} orbitals. This electronic configuration results in $A_{hf}^{dip} = 0$.[17] For a free Co^{2+} ion, the d-core polarization coupling constant is -105 kOe/μ_B.[20] Due to quenching of the orbital angular momentum L_z, there is no finite contribution of the L_z in the first order. But if we consider the second-order perturbation of the spin-orbit interaction, the orbital quenching is partially lifted. This contribution due to the spin-orbit coupling has a positive sign and is estimated to be 85.1 kOe/μ_B for Co^{2+} ions at the tetrahedral sites.[17] From Eq. (7), we obtain

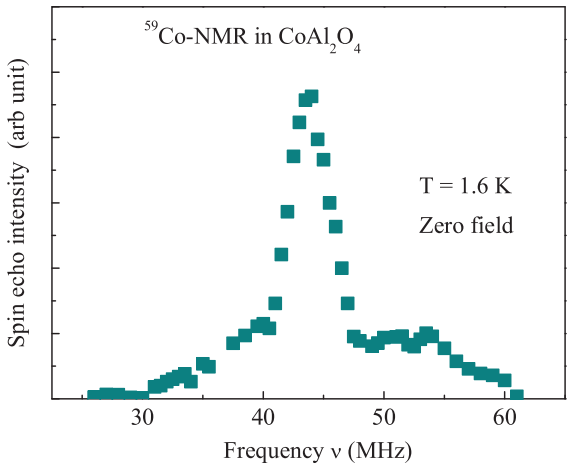

FIG. 13. (Color online) Zero-field ^{59}Co-NMR spectrum under zero external field at 1.6 K.

$A_{hf} = -19.9$ kOe/μ_B, which can reasonably explain the experimental value of $-18.0(5)$ kOe/μ_B.

The temperature-independent orbital part of the NMR shift for the Co^{2+} at the A site is estimated to be $K_{orb} = 5.46(3)\%$ from the K-χ analysis. The K_{orb} relates to Van Vleck susceptibility χ_{VV} for Co^{2+} at the A site as $K_{orb} = \frac{A_{orb}}{N_A}\chi_{VV}$ where A_{orb} is the orbital hyperfine coupling constant given by[21]

$$A_{orb} = 2\mu_B \left\langle \frac{1}{r^3} \right\rangle. \quad (8)$$

Here, $\langle \frac{1}{r^3} \rangle$ is an average of $\frac{1}{r^3}$ over $3d$ electrons. Using $\langle \frac{1}{r^3} \rangle = 6.02$ a.u. for Co^{2+} (Ref. 22), χ_{VV} is estimated to be $4(2) \times 10^{-4}$ cm^3/mol which is in good agreement with T-independent magnetic susceptibility discussed in Sec. IV.

Below T_N, we observe a NMR signal of Co nuclei at the A site under zero magnetic field, which again confirms long-range magnetic ordering. Figure 13 shows the zero-field ^{59}Co-NMR spectrum at 1.6 K. A similar zero-field ^{59}Co-NMR spectrum at the A site has been previously reported for the spinel compound Co_3O_4 in the AFM state.[17] The resonance frequency $\nu_0 = 43.5(4)$ MHz at the peak intensity point is lower than $\nu_0 = 55.7$ MHz in Co_3O_4.[17] The internal field H_{int} at the Co A site is evaluated to be 43.3(4) kOe at 1.6 K. With the value of $A_{hf} = -18.0$ kOe/μ_B deduced from the K-χ plot, the ordered moment $\langle\mu\rangle$ of Co^{2+} is estimated to be 2.4(1) μ_B/Co using the relation $H_{int} = |A_{hf}|\langle\mu\rangle$. This value is smaller than the expected value of 3 μ_B/Co for $S = \frac{3}{2}$ of Co^{2+} ions with $g = 2$ and is larger than the value of 1.58 μ_B/Co reported from the ND study done previously by Zaharko *et al.*[3] The shoulderlike structures of the spectrum are due to a distribution of Co^{2+} spin moments in the AFM state.

C. ^{27}Al spin-lattice relaxation rates

In order to investigate the dynamical behavior of the Co^{2+} spins in $CoAl_2O_4$, ^{27}Al spin-lattice relaxation rates $(1/T_1)$ were measured at different temperatures. In the case of ^{27}Al ($I = \frac{5}{2}$), the nuclear magnetization recovery of the central transition after a $\pi/2$ saturation pulse is given by[23]

$$\frac{M(\infty) - M(t)}{M(\infty)} = (0.029e^{-t/T_1}) + (0.18e^{-6t/T_1}) + (0.79e^{-15t/T_1}), \quad (9)$$

where $M(t)$ is the nuclear magnetization at time t after the saturation pulse. The experimental recovery curves above T_N were well fitted by the equation, while below T_N the equation could not fit the experimental data due to distributions of T_1. The distributions of T_1 are mainly due to the inhomogeneous broadening of the ^{27}Al-NMR spectrum in our powder sample and also due to the distribution of the Co^{2+} spin moments in the AFM state. Then, we tentatively assumed that the experimental recovery curve is composed of two components, one with a short relaxation time T_{1S} and another with long relaxation time T_{1L} and we carried out a fit using the following equation:

$$\frac{M(\infty) - M(t)}{M(\infty)} = M_S[(0.029e^{-t/T_{1S}}) + (0.18e^{-6t/T_{1S}}) + (0.79e^{-15t/T_{1S}})] + M_L[(0.029e^{-t/T_{1L}}) + (0.18e^{-6t/T_{1L}}) + (0.79e^{-15t/T_{1L}})], \quad (10)$$

where $M_S + M_L = 1$. The temperature dependence of M_S is shown in the inset of Fig. 14. We also estimated T_1 below T_N by fitting the experimental recovery data with a stretched exponential function. The $1/T_1$ shows a similar temperature dependence to those of $1/T_{1S}$ and $1/T_{1L}$ below T_N.

Figure 14 shows the temperature dependence of $1/T_{1S}$ and $1/T_{1L}$. With decreasing T, $1/T_{1S}$ decreases and shows a minimum around 50 K and exhibits a sharp peak at $T = 10.0(5)$ K. The sharp peak of $1/T_1$ is due to critical slowing down of spin fluctuations expected for a second-order phase transition, which again confirms the AFM long-range magnetic ordering at T_N. Below 10 K, $1/T_1$ rapidly falls and then decreases slowly where both $1/T_{1S}$ and $1/T_{1L}$ show

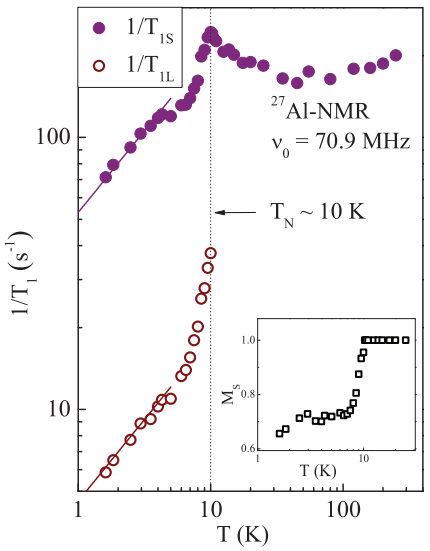

FIG. 14. (Color online) T dependence of the short and long nuclear spin-lattice relaxation rates $1/T_{1S}$ and $1/T_{1L}$, respectively. Below 4 K, both $1/T_{1S}$ and $1/T_{1L}$ show $T^{0.6}$ power-law behavior shown by the solid lines. The inset shows the T dependence of M_S which corresponds to the fraction of $1/T_{1S}$ defined in Eq. (10).

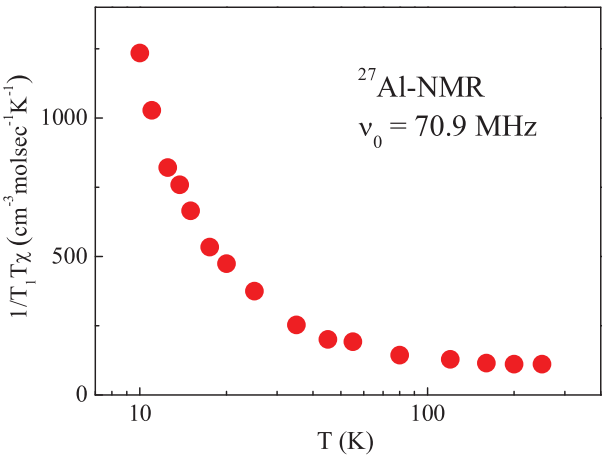

FIG. 15. (Color online) $1/T_1T\chi$ versus temperature T for a resonance frequency of 70.9 MHz. $1/T_1T\chi$ increases with decreasing temperature indicating the growth of AFM spin correlations.

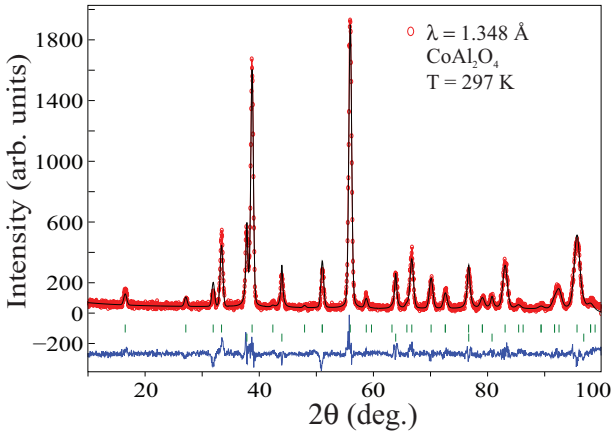

FIG. 16. (Color online) Neutron diffraction intensity versus scattering angle 2θ at room temperature (red circles) and the calculated refined pattern (solid black line). The vertical green tick marks indicate the peak positions of Bragg reflections and the lower blue line shows the difference between the model calculations and measured data.

$T^{0.6}$ power-law behavior (shown by the straight lines in the figure) below 4 K. In the antiferromagnetically ordered state, $1/T_1$ is mainly driven by scattering of magnons, leading to T^3 or T^5 power-law temperature dependencies due to a two- or three-magnon Raman process, respectively. The weak T dependence of $1/T_1 \sim T^{0.6}$ below 4 K can not be explained by the magnon scattering, and suggests the presence of other magnetic fluctuations in the magnetically ordered state, which could originate from spin frustrations and/or short-range magnetic correlations revealed by the neutron scattering measurements described in the following.

In order to see spin fluctuation effects in the paramagnetic state, it is useful to replot the data by changing the vertical axis from $1/T_1$ to $1/T_1T\chi$ as shown in Fig. 15. $1/T_1T$ can be expressed in terms of the imaginary part of the dynamic susceptibility $\chi''(\vec{q},\omega_0)$ per mole of electronic spins as[24,25]

$$\frac{1}{T_1T} = \frac{2\gamma_N^2 k_B}{N_A^2}\sum_{\vec{q}}|A(\vec{q})|^2\frac{\chi''(\vec{q},\omega_0)}{\omega_0}, \qquad (11)$$

where the sum is over the wave vectors $\vec{q}$ within the first Brillouin zone, $A(\vec{q})$ is the form factor of the hyperfine interactions, and $\chi''(\vec{q},\omega_0)$ is the imaginary part of the dynamic susceptibility at the Larmor frequency ω_0. On the other hand, the uniform χ corresponds to the real component $\chi'(\vec{q},\omega_0)$ with $q = 0$ and $\omega_0 = 0$. Thus, a plot of $1/T_1T\chi$ versus T shows the T dependence of $\sum_{\vec{q}}|A(\vec{q})|^2\chi''(\vec{q},\omega_0)$ with respect to that of the uniform susceptibility $\chi'(0, 0)$. For high temperatures above 100 K, $1/T_1T\chi$ is a nearly constant showing that the temperature dependence of $\sum_{\vec{q}}|A(\vec{q})|^2\chi''(\vec{q},\omega_0)$ scales to that of $\chi'(0, 0)$. On the other hand, with decrease in temperature, $1/T_1T\chi$ starts to increase below 100 K which is $\sim$10 times higher than T_N. The increase of the $1/T_1T\chi$ at $T \gg T_N$ can not be simply attributed to the critical slowing down of spin fluctuations near T_N. This implies $\sum_{\vec{q}}|A(\vec{q})|^2\chi''(\vec{q},\omega_0)$ increases more than $\chi'(0, 0)$, which is due to a growth of spin fluctuations with $q \neq 0$, most likely with AFM wave vector $q = Q_{AF}$, even at T much higher than T_N. Thus, we conclude that strong AFM spin fluctuations are realized in a wide temperature region up to $\sim$100 K in the paramagnetic state.

VII. NEUTRON DIFFRACTION

Analysis of a powder neutron diffraction pattern taken at room temperature (Fig. 16) is consistent with a single $Fd\bar{3}m$ phase of $CoAl_2O_4$. Due to the relatively small difference in the neutron coherent scattering lengths between Al and Co, the Rietveld refinement of the powder diffraction pattern is not sensitive to the Co-Al site inversion discussed in Sec. III.

A prominent (002) reflection, not allowed by the chemical structure, emerges below 10 K as shown in Fig. 17(a) and its intensity increases upon cooling to the base temperature of 3 K. Measurable intensity increases are also observed for the (111), (113), (222), and (133) nuclear Bragg reflections between scans taken at 15 and 3 K (not shown). Whereas the (002) peak is slightly broader than the Bragg peaks in its vicinity, the (111) magnetic peak is much broader than the (111) nuclear peak, in agreement with similar observations of single crystals.[3,8] The unusual broadening along the (111) reflection (reported for a single crystal[3]) makes the observation of the (222) reflection virtually impossible with the small amount of sample we used in this study. The emergence of the (002) and the increase in intensities of the Bragg reflections, that fall off systematically with the increase in 2θ (due to magnetic form factor), are consistent with long-range AFM ordering of the Co spins at the A sites with a magnetic space group $F\bar{4}3m$. Based on the temperature dependence of the integrated intensity of the (002) [see Fig. 17(b)], T_N is estimated to be 10.3(9) K, which is in agreement with the value estimated from NMR and specific-heat measurements within experimental uncertainty. The diamond structure of Co^{2+} consists of two interpenetrating fcc sublattices, with origins at (0,0,0) (spin up) and at $(\frac{1}{4},\frac{1}{4},\frac{1}{4})$ (spin down), as shown in the inset of Fig. 17(b). The four spins in one sublattice are parallel to the [001] direction and the other four in the other sublattice are antiparallel to those. This AFM structure is similar to that observed for the A site

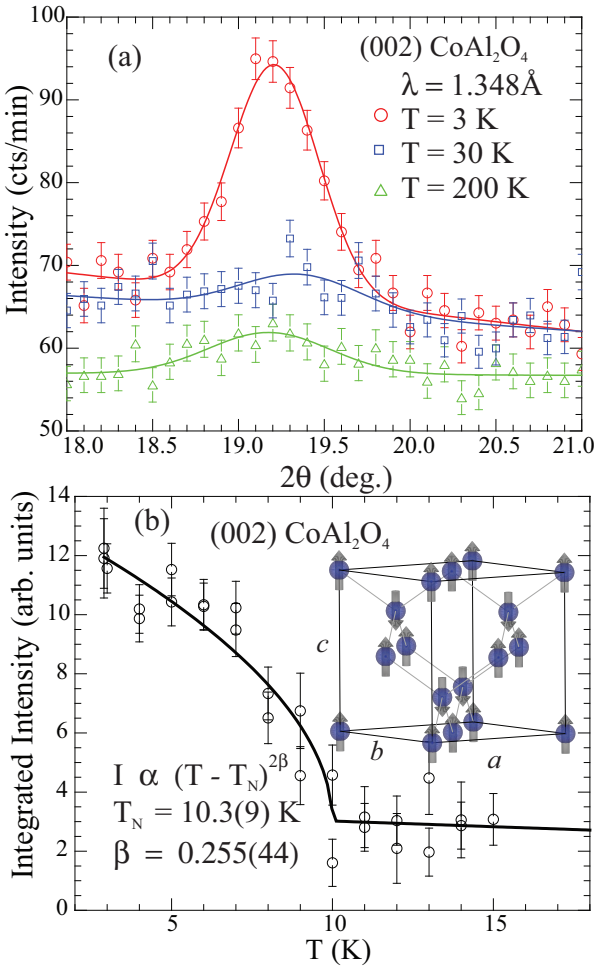

FIG. 17. (Color online) (a) Intensity versus scattering angle (2θ) of the (002) magnetic reflection at various temperatures demonstrating the long-range magnetic order. Temperature dependence of background in the 2θ range shown in (a) indicates possible short-range magnetic order above T_N. The weak peak above the transition is nonmagnetic in origin [most likely due to a strong nuclear (004) reflection by $\lambda/2$ contamination in the beam] and persists to room temperature. (b) Integrated intensity of the (002) as a function of temperature. The solid line is a fit to a power law with $T_N = 10.3(9)$ K and $\beta = 0.255(44)$. Inset: Antiferromagnetic structure below T_N where the spin direction is arbitrary. Magnetic and crystallographic unit cell are same with $a = b = c$.

of Co^{2+} in Co_3O_4, for which an average magnetic moment 3.26 μ_B/Co at 4.2 K was obtained from ND analysis.[26] Our detailed analysis of the magnetic diffraction pattern yields a 1.9(5) μ_B/Co average ordered magnetic moment, lower than 3 μ_B/Co expected for Co^{2+} ($S = \frac{3}{2}$, $g = 2$), in agreement with 2.4(1) μ_B/Co from the above NMR measurements within errors.

We emphasize that our collinear AFM model is consistent with our experimental observations, although it may not be unique as is the general case in any diffraction analysis. We have, however, explored a few noncollinear models and the picture that emerges is that they lead to extra reflections that either are not observed experimentally or are too weak to detect with our powder sample. In particular, they lead to

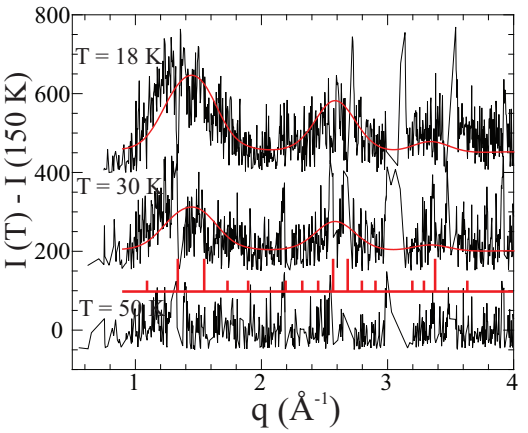

FIG. 18. (Color online) Elastic neutron scattering intensity versus scattering wave vector q at various temperatures above T_N, as indicated, after subtraction of a similar scan at $T = 150$ K. The broad peaks at 18 and 30 K are evidence for short-range AFM order that persists up to about $T = 50$ K. Sharp spikes in the subtracted patterns are due to temperature shifts of prominent nuclear Bragg reflections. Solid lines are calculated magnetic diffraction patterns assuming the underlying magnetic structure shown in Fig. 17(b) with 6% random Co^{2+} vacancies. The marks show the calculated diffraction peaks that contribute to the pattern; the longer marks indicate prominent reflections that appear below T_N and the shorter ones correspond to weaker peaks that appear as a result of vacancies.

lowest-order reflection (001) that is not observed. The lowest-order vector observed in our diffraction study is the (002) indicating this is the propagation vector of the AFM structure. Most notably, our careful search for a spin-spiral magnetic ordering as discussed in Refs. 2 and 27 produced a null result, i.e., the satellite peaks associated with the spin-spiral state were found to be absent, demonstrating that, at least for the particular value of the inversion parameter in this work and to within our sensitivity limits, there is not a spin-spiral state present.

Figure 18 shows the diffraction intensity versus momentum transfer [$q = 4\pi \sin(\theta)/\lambda$] at three temperatures above T_N after subtracting a similar data set taken at higher $T =$ 150 K. The patterns indicate remnant dynamic short-range order (SRO) above the transition that disappears between 30 and 50 K. The pattern, shown in Fig. 18 at $T = 18$ K, is very similar to that observed by Krimmel *et al.*[28] at $T =$ 1.6 K for a sample with 6%–8% site inversion which does not show long-range magnetic ordering down to 1.6 K. In order to see the effects of the site inversion on the short-range magnetic ordering, we have calculated the q dependence of the intensity by assuming 6% random Co^{2+} vacancies in a unit cell. In the calculation, we assumed the magnetic structure at the base temperature with the 6% random vacancies, and allowed for uniform broadening of all magnetic peaks beyond the spectrometer's resolution. The calculated results shown by solid lines in Fig. 18 reasonably reproduce the observed patterns. This suggests that the SRO above T_N originates mainly from the site inversion effects. It is known that the site inversion can be as high as 22% (Ref. 29), and such high inversion can eventually lead to a complete suppression of long-range magnetic ordering.[10,28] In this regard, it is

interesting to note that the AFM transition temperature for Co_3O_4, associated with the ordering of the Co^{2+} A site, is at $T_N \approx 30$–40 K,[1,6,17,26] which is very close to the temperature at which the SRO disappears in our sample. In view of the site inversion playing a major role in determining T_N, it is likely that reducing the inversion will enhance T_N in $CoAl_2O_4$. Of course, T_N will also be controlled by the spin frustration which has been pointed out to play an important role in the system. To investigate the effect of spin frustration due to next-nearest-neighbor exchange coupling (J_2) in detail, one needs an inversion-free $CoAl_2O_4$ sample, although so far no one has obtained such a sample, with the lowest value of inversion parameter being at $x \approx 0.02(4)$.[8] Another candidate to study spin frustration effects in A-site spinels would be Co_3O_4 where the likelihood for Co^{2+}-Co^{3+} inversion is negligible, with the B site occupied by the nonmagnetic Co^{3+}. However, since the ratio of the exchange coupling constants for Co_3O_4 is $J_2/J_1 = 0.019$ (with $J_1 = 1.09$ meV and $J_2 = 0.02$ meV) (Ref. 3) which is almost six times smaller than 0.109 for $CoAl_2O_4$ (Ref. 3), one expects much weaker spin frustration effects in Co_3O_4.

VIII. SUMMARY AND CONCLUSIONS

Our $C_p(T)$, NMR, and ND data clearly demonstrate that $CoAl_2O_4$ exhibits a collinear AFM ground state below $T_N = 9.8(2)$ K. The ^{27}Al-NMR spectrum exhibits a symmetric broadening below 10 K which indicates the presence of a long-range AFM-ordered ground state for this compound. Furthermore, the linewidth of the NMR spectrum which is proportional to the order parameter shows a continuous increase below 10 K, as expected for second-order phase transition. The presence of spontaneous magnetization below 10 K is confirmed directly by the observation of a ^{59}Co NMR signal under zero magnetic field in the magnetically ordered state. Using the internal field at the Co sites in the magnetically ordered state and the hyperfine coupling constant estimated from the K-χ analysis, an ordered moment at the A-site Co^{2+} ion is estimated to be 2.4(1) μ_B/Co. The sharp peak of $1/T_1$ at around 10 K further confirms a second-order phase transition to a long-range magnetically ordered state at the same temperature. The results from the ND measurements are not only consistent with the NMR results but also indicate a collinear long-range AFM-ordered ground state for this compound with an ordered moment of 1.9(5) μ_B/Co, consistent with the estimate from NMR.

The magnetic entropy variation ΔS_{Mag} at 100 K is $\approx$11% smaller than the expected saturation value of 10.9 J/mol K, suggesting a nonzero magnetic entropy at $T = 0$ K. ΔS_{Mag} at T_N is considerably smaller than its value at high temperature, which indicates that strong AFM correlations occur above T_N. The emergence of AFM correlations was manifested by the increase of $1/T_1T\chi$ below 100 K, by the presence of broad magnetic peaks observed below 50 K in the ND measurements, and by the broad peak in $\chi(T)$ at $\approx$15 K.

There are two factors which govern the magnetic properties of this system, viz., frustration and site inversion. We successfully prepared a polycrystalline sample of $CoAl_2O_4$ with a low inversion parameter $x = 0.057(20)$. Site disorder creates increased randomness of exchange interactions in the already frustrated compound.[10] The suppression of the value of magnetic entropy at high temperatures from the value expected for $S = \frac{3}{2}$ suggests that the effective spin of the Co at the A site is smaller than $\frac{3}{2}$, which could be a manifestation of both spin frustration and Co-Al site inversion effects. The presence of dynamic short-range magnetic ordering observed in neutron scattering experiments below $\sim$50 K can be caused mainly by the site inversion effects. As pointed out previously, although a spin-liquid ground state has been proposed from magnetic susceptibility measurements for $CoAl_2O_4$ with low values of x,[6,10] our NMR and ND measurements conclusively proved the existence of a long-range AFM-ordered state below 10 K. Since site inversion plays a crucial role in determining the magnetic properties of this spinel compound, it will also be interesting to perform systematic NMR and ND measurements on highly disordered (high-x) $CoAl_2O_4$ samples to investigate how the system changes from the AFM state to a spin-glass state.

ACKNOWLEDGMENTS

We thank V. Tsurkan for providing us the heat-capacity data of the nonmagnetic reference compound $ZnAl_2O_4$ in Ref. 9. This research was supported by the US Department of Energy, Office of Basic Energy Sciences, Division of Materials Sciences and Engineering. Ames Laboratory is operated for the US Department of Energy by Iowa State University under Contract No. DE-AC02-07CH11358.

[1] W. L. Roth, J. Phys. (Paris) **25**, 507 (1964).
[2] D. Bergman, J. Alicea, E. Gull, S. Trebst, and L. Balents, Nat. Phys. **3**, 487 (2007).
[3] O. Zaharko, N. B. Christensen, A. Cervellino, V. Tsurkan, A. Maljuk, U. Stuhr, C. Niedermayer, F. Yokaichiya, D. N. Argyriou, M. Boehm, and A. Loidl, Phys. Rev. B **84**, 094403 (2011).
[4] N. Tristan, J. Hemberger, A. Krimmel, H.-A. Krug von Nidda, V. Tsurkan, and A. Loidl, Phys. Rev. B **72**, 174404 (2005).
[5] A. P. Ramirez, Annu. Rev. Mater. Sci. **24**, 453 (1994).
[6] T. Suzuki, H. Nagai, M. Nohara, and H. Takagi, J. Phys.: Condens. Matter **19**, 145265 (2007).
[7] O. Zaharko, A. Cervellino, V. Tsurkan, N. B. Christensen, and A. Loidl, Phys. Rev. B **81**, 064416 (2010).
[8] G. J. MacDougall, D. Gout, J. L. Zarestky, G. Ehlers, A. Podlesnyak, M. A. McGuire, D. Mandrus, and S. E. Nagler, Proc. Natl. Acad. Sci. USA **108**, 15693 (2011).
[9] N. Tristan, V. Zestrea, G. Behr, R. Klingeler, B. Büchner, H.-A. Krug von Nidda, A. Loidl, and V. Tsurkan, Phys. Rev. B **77**, 094412 (2008).
[10] K. Hanashima, Y. Kodama, D. Akahoshi, C. Kanadani, and T. Saito, J. Phys. Soc. Jpn. **82**, 024702 (2013).
[11] J. Rodríguez-Carvajal, Phys. B (Amsterdam) **192**, 55 (1993); see also www.illeu/sites/fullprof/.

[12] A. Maljuk, V. Tsurkan, V. Zestrea, O. Zaharko, A. Cerellino, A. Loidl, and D. N. Argyriou, J. Cryst. Growth. **311**, 3997 (2009).
[13] M. Hagiwara, S. Kimura, N. Nishihagi, T. Suzuki, M. Nohara, H. Takagi, and K. Kindo, J. Low Temp. Phys. **159**, 11 (2010).
[14] D. Meschede, F. Steglich, W. Felsch, H. Maletta, and W. Zinn, Phys. Rev. Lett. **44**, 102 (1980).
[15] L. R. Walker and R. E. Walstedt, Phys. Rev. Lett. **38**, 514 (1977).
[16] K. Miyatani, K. Kohn, S. Iida, and H. Kamimura, J. Phys. Soc. Jpn. **20**, 471 (1965).
[17] T. Fukai, Y. Furukawa, S. Wada, and K. Miyatani, J. Phys. Soc. Jpn. **65**, 4067 (1996).
[18] T. Tsuda, A. Hirai, and H. Abe, Phys. Lett. A **26**, 463 (1968).
[19] Y. Furukawa, S. Wada, T. Kajitani, and S. Hosoya, J. Phys. Soc. Jpn. **68**, 346 (1999).
[20] A. Abragam, J. Horowitz, and M. H. L. Pryce, Proc. R. Soc. London, Ser. A **230**, 169 (1955).
[21] A. Narath, in *Hyperfine Interactions*, edited by A. J. Freeman and R. B. Frankel (Academic, New York, 1967).
[22] A. J. Freeman and R. E. Watson, in *Magnetism*, edited by G. T. Rado and H. Shul (Academic, New York, 1965), Vol. 2.
[23] A. Narath, Phys. Rev. **162**, 320 (1967).
[24] T. Moriya, J. Phys. Soc. Jpn. **18**, 516 (1963).
[25] A. V. Mahajan, R. Sala, E. Lee, F. Borsa, S. Kondo, and D. C. Johnston, Phys. Rev. B **57**, 8890 (1998).
[26] W. L. Roth, J. Phys. Chem. Solids **25**, 1 (1964).
[27] J. S. Bernier, M. J. Lawler, and Y. B. Kim, Phys. Rev. Lett. **101**, 047201 (2008).
[28] A. Krimmel, V. Tsurkan, D. Sheptyakov, and A. Loidl, Phys. B (Amsterdam) **378-380**, 583 (2006).
[29] A. Nakatsuka Y. Ikeda, Y. Yamasaki, N. Nakayama, and T. Mizota, Solid State Commun. **128**, 85 (2003).